applied sciences

MDPI

Article

TLS and GB-RAR Measurements of Vibration Frequencies and Oscillation Amplitudes of Tall Structures: An Application to Wind Towers

Serena Artese [1,2,*] and Giovanni Nico [3,4]

1 Department of Civil Engineering, University of Calabria, 87036 Rende (CS), Italy
2 Spring Research s.r.l., University of Calabria, 87036 Rende (CS), Italy
3 Istituto per le Applicazioni del Calcolo, Consiglio Nazionale delle Ricerche, 70126 Bari, Italy; g.nico@ba.iac.cnr.it
4 Institute of Earth Sciences, Saint Petersburg State University, 199034 Saint Petersburg, Russia
* Correspondence: serena.artese@unical.it

Received: 5 March 2020; Accepted: 23 March 2020; Published: 25 March 2020



Abstract: This article presents a methodology for the monitoring of tall structures based on the joint use of a terrestrial laser scanner (TLS), configured in line scanner mode, and a ground-based real aperture radar (GB-RAR) interferometer. The methodology provides both natural frequencies and oscillation amplitudes of tall structures. Acquisitions of the surface of the tall structure are performed by the TLS with a high sampling rate: each line scan provides an instantaneous longitudinal section. By interpolating the points of each line, oscillation profiles are estimated with a much better precision than each single point. The amplitude and frequency of the main oscillation mode of the whole structure are derived from the TLS profiles. GB-RAR measurements are used to measure the vibration frequencies of higher oscillation modes which are not caught by the TLS due its lower precision in the measurement of displacements. In contrast, the high spatial resolution of TLS measurements provides an accurate description of oscillation amplitude along the tower, which cannot be caught by the GB-RAR, due to its poorer spatial resolution. TLS and GB-RAR acquisitions are simultaneous. The comparison with the analytical solution for oscillation modes demonstrates that the proposed methodology can provide useful information for structural health monitoring (SHM). The methodology does not require the use of targets on the structure and it can be applied during its normal use, even in presence of dynamic loads (wind, traffic vibrations, etc.). A test was carried out on a wind tower where the synergistic use of TLS and GB-RAR made it possible to fully describe the spectral properties of the tower and at the same time measure the amplitude of the first oscillation mode along the tower with a high spatial resolution.

Keywords: terrestrial laser scanner (TLS); ground-based real aperture radar (GB-RAR); line scanner; vibration frequency; spectral analysis; displacement; structural health monitoring (SHM)

1. Introduction

In the last decade, a growing sensitivity has developed towards problems related to the integrity of structures, both in the construction sector and in that of road and railway infrastructures, as well as in that of industrial plants and products.

To check the functionality and health of these structures, natural vibration frequencies and oscillation amplitudes are among the most important parameters. This is even truer for slender or tall structures, such as very tall buildings, piles and spars of bridges and towers. For this kind of structure, it is mandatory to know the behavior when dynamic loads are applied (e.g., strong winds, vibrations due to traffic, earthquake-induced shaking). The ever more widespread presence of tall structures in

urbanized and even densely inhabited areas makes their control more useful, which also helps avoid risks to the safety of people. For this reason, the development of simple methodologies for the quick inspection of slender or tall structures is of interest for SHM.

Wind towers are high cantilever structures, which are subject at one end to strong horizontal loads and cyclical stresses due to the rotors; these stresses are reflected in particular on the foundations and on the foundation soil. Thus, for these structures, the control of the frequencies is of fundamental importance.

Several techniques have been adopted for SHM [1]. Among these, techniques based on the measurement of the structural vibration are increasingly used; a review of vibration-based methods can be found in [2,3]. Among the various techniques proposed for measuring the frequencies of structures, those based on the acquisition of accelerometers and velocimeters have been widely used for decades [4,5]. The use of micro-electro-mechanical systems (MEMS)-based sensors and wireless connected sensors is growing, in order to set up even very dense control networks [6,7]. Global navigation satellite system (GNSS) receivers offer the possibility of extracting vibration frequencies [8]; as for the aforementioned techniques, the limit of GNSS is the point-like property of its measurements; moreover, it is necessary to position the GNSS receiver on the point to be monitored. Total stations (TS) are also used, thanks to their increased sampling rate [9] and the possibility of performing long-range monitoring with high precision using appropriate atmospheric correction techniques [10]. Another non-contact technique, continuously growing thanks to the increasing resolution of charge-coupled devices (CCD) and complementary metal–oxide–semiconductor (CMOS) sensors, and to the high frame rate of the most recent cameras, is based on photogrammetry and image processing [11,12].

Ground-based real aperture radar (GB-RAR) offers the possibility to monitor the dynamic characteristics of the structures while ensuring, at the same time, precise measurements of vibration frequencies and displacements. This long-range, non-contact methodology is even more widely adopted for monitoring large structures, for post-disaster interventions and for SHM [13–18].

TLS is a recent technique, still in the evolution phase, used in a wide range of applications and in particular for structural monitoring. Its strength lies in its ability to acquire a very large number of points in a short time, thus making it possible to survey even very complex objects, and to obtain detailed 3D models, thanks to point cloud processing software that is increasingly evolved. TLS, usually mounted on a tripod in fixed positions, is mainly used to monitor the deformations of the structures by measuring the differences between the surfaces scanned at different times [19]. In the last decade, several TLS applications can be counted for the monitoring of dynamic phenomena and the measurement of structure vibrations. Kim and Kim [20] used a Riegl VZ-400® to perform dynamic displacement measurement. The smoothing of the acquired data was performed by using a kriging approach. Two experimental tests were conducted in laboratory on a small object and under ideal conditions. Neitzel et al. [21] showed a comparison between a TLS and a sensor system based on low cost MEMS accelerometers for measuring the vibrations of a bridge. They used a Zoller + Froehlich Imager 5003® in 1D mode; thus, measurements were performed on a single point. A GB-RAR was used for reference purposes. In this case, the accelerometers showed a better accuracy than TLS.

Schill and Eichhorn investigated the movements and frequencies of two wind towers. For each test, they used two Zoller+Fröhlich® 9012 profilers, with sight lines on the rotor plane and perpendicular to it [22].

In this work, a technique is proposed for the measurement of natural vibration frequencies and oscillation amplitudes of structures, based on the TLS acquisition of scan lines and GB-RAR interferometry. The technique used to process the TLS acquisitions, in order to obtain a better precision than the instrumental one, is explained. A test is carried out on a wind tower and data is acquired both during normal activity and during the deactivation phase of the wind turbine. The frequencies and the oscillation amplitudes obtained from the processing of the collected data are compared with the theoretical ones, resulting from an analytical solution. A comparison is made with the results

obtained by GB-RAR, which acquires data simultaneously with the TLS. The results obtained, and the comparison with the theoretical solution and with GB-RAR, are shown also through figures and tables and the synergistic use of the two instruments is discussed.

The structure of the article is as follows: Section 2 introduces the TLS technique in line scanner mode and the technique used for data processing, in order to optimize the results, along with a brief introduction to the GB-RAR technique. Section 3 shows the test results. Section 4 provides discussion of the results. Finally, in Section 5, some conclusions are drawn.

2. Materials and Methods

This section introduces the basic principles of TLS and GB-RAR techniques and describes the proposed methodology to measure the vibration frequencies and the oscillation amplitudes of a tall structure, with particular reference to wind towers.

2.1. TLS Basic Principles

TLS is a non-destructive testing (NDT) technique based on the emission of a laser beam of known direction, used to quickly measure the position of points on the surface of a surveyed object, in a reference system with the origin in the center of the instrument. Two principles are adopted to measure distances: time-of-flight (ToF) and phase shift. In our case, a TLS ToF is used. Figure 1 illustrates the operating principle of the ToF. A short pulse is emitted by the TLS through a photodiode. The distance is obtained through the ToF of the emitted impulse, which is the time interval Δt taken by the impulse to reach a target and go back. Then, the distance d from TLS to target is given by Equation (1):

$$d = \frac{c\Delta t}{2} \tag{1}$$

where c is the speed of light.

As for the direction of the laser beam, this is obtained by the scanning system, usually consisting of a multi-facet mirror that rotates around a horizontal axis for vertical scanning, while the entire instrument rotates around a vertical axis through a motor, like the alidade of a motorized TS. In the case of a line scanner configuration, rotation around the vertical axis is disabled. The maximum range can reach 6000 m, while the attainable precision for single points varies from 1 to 20 mm. Better values are obtained for shorter distances [23].

For our application, we made use of a TLS Riegl VZ-1000®, RIEGL Laser Measurement Systems GmbH, Horn, Austria, whose characteristics are summarized in Table 1.

Table 1. Characteristics of TLS Riegl VZ-1000®.

Accuracy of Single Point	**± 8 mm**
Precision of single point	± 5 mm
Range	from 1 m to 1400 m.
Sampling frequency	until 122.000 points/sec.
Field of view	100° (Vertical +60° −40°)/360° (Horizontal).
Scan Speed	3 lines/sec to 120 lines/sec
Angular Stepwidth	0.0024° to 0.288° between consecutive shoots
Angle Measurement Resolution	0.0005° (1.8 arcsec)
Timestamp	Yes

The Riegl VZ 1000® TLS is a versatile instrument. Along with the possibility to operate in line scan mode, it makes it possible to perform long-range surveys and, therefore, to obtain 3D models of objects and of the surrounding environment.

When line scan mode is selected, the laser beam describes a line repeatedly, being addressed only by the multi-faceted mirror (see Figure 1). Using the maximum scanning speed of 120 lines per second,

it would be theoretically possible to measure vibration frequencies up to 60 Hz. Taking into account the precision of measurement, it is necessary to consider a strong noise in the time series of samples, which would make it very difficult to measure oscillations with a peak-to-peak difference less than 1 cm. This limit can be overcome if information on the geometry of the surveyed object is used.

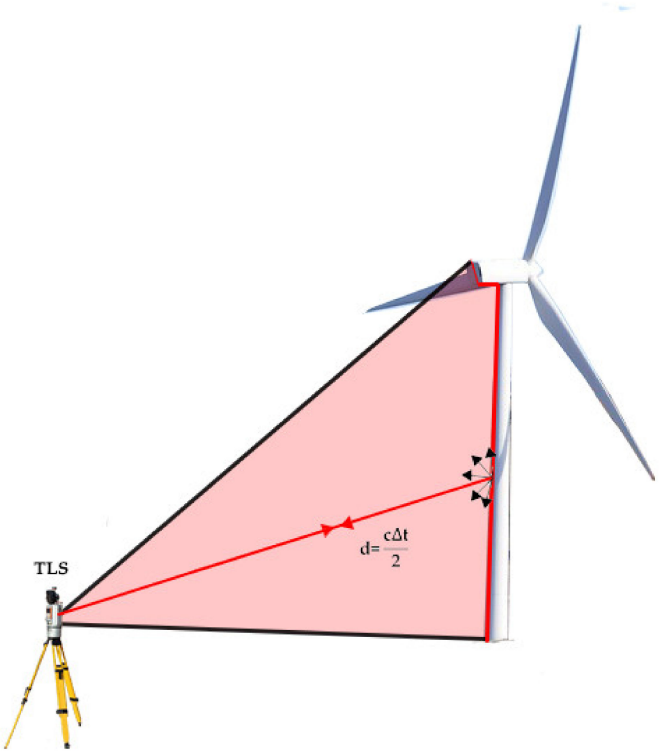


Figure 1. Sketch of the TLS functioning in line scan mode. The distance d is computed in Equation (1).

2.2. GB-RAR Basic Principles

A ground-based real aperture radar (RAR) system is a stepped-frequency continuous-wave (SF-CW) radar that emits a continuous wave with different progressive frequencies within a given frequency band. The frequency bandwidth B provides the range resolution ΔR of the radar according to the relationship, Equation (2):

$$\Delta R = \frac{c}{2B} \tag{2}$$

where c is the speed of electromagnetic waves in vacuum. The corresponding echoes, backscattered by the scene, give rise to the raw data. Table 2 summarizes the main technical specifications of the IBIS-F/L® GB-RAR, IDS S.p.a, Pisa, Italy, used in this experiment.

The inverse Fourier transform of the raw signal acquired by the radar, normalized and converted to a logarithmic scale, provides the normalized radar cross-section (NRCS) profile, which shows the amplitude of the radar signal backscattered by targets located within the scene, discriminating them with the range resolution (2).

The interferometric phase is computed as follows:

$$\Delta\varphi_{1,2} = \text{atan}\{S_2 \cdot conj(S_1)\} \tag{3}$$

where S1 and S2 are two coherent complex-values radar data acquired at times t_1 and t_2, respectively, during the data acquisition. The line-of-sight (LoS) displacement $D_{1,2}$ of a point P, occurring in the time interval [t_1, t_2], is related to the interferometric phase $\Delta\varphi_{1,2}$, computed in Equation (3), by the relationship:

$$D_{1,2} = \frac{\lambda}{4\pi}\Delta\varphi_{1,2} \quad (4)$$

where λ is the radar wavelength. The precision of displacement measurements depends on the precision of phase measurements and it is a fraction of millimeter.

In the case of RAR interferometric applications, the radar acquires data with a sampling time in the order of a fraction of second, usually of a few milliseconds. This means that the radar can accurately track in time the deformation profile of the target. The vibration frequency spectrum is obtained by a spectral analysis of the displacement profile, computed in Equation (4). The vibration frequency spectra can be visualized as 2D maps. For each target, discriminated in range with a range resolution ΔR, the frequency spectra and displacement profiles are displayed vs. frequency and time, respectively.

Table 2. Technical Specifications of IBIS-F/L GB-RAR.

Range Resolution	**0.75 m**
Central frequency	17.2 GHz
Frequency bandwidth B	200 MHz

2.3. Methodology

This section describes the methodology proposed in this paper for the accurate characterization of dynamical behavior of tall structures. The methodology goes through the following steps:

(1) Co-location of TLS and GB-RAR in the same local reference system, and high-resolution geometric survey of the tall structure by TLS, for the co-registration of TLS and GB-RAR measurements;
(2) Model-based processing of TLS data acquired in line-scan mode, to increase the precision of TLS displacement measurements and consequent estimation of displacements and frequencies of oscillation modes having an amplitude lower than the precision achieved by TLS measurements;
(3) Interferometric processing of GB-RAR data, with 2D visualization of the frequency spectra of the structure oscillations.

The comparison and integration of TLS-based vibration frequencies with those provided by GB-RAR makes it possible to identify instrument artifacts and to extend measurements to higher oscillation modes, with an amplitude smaller than the enhanced TLS precision attained at point (2).

Below, we will examine the previous points to describe in detail each step of the proposed methodology applied to a wind tower.

2.3.1. Co-Location of TLS and GB-RAR Instruments and Co-Registration of Their Measurements

The co-location of TLS and GB-RAR is carried out by a TS topographic survey providing the coordinates of the TLS and GB-RAR, as well as of the base of the wind tower in the same local reference system. Figure 2 shows the layout of the TS survey (a) and a sketch of the local reference system with the positions of the TS, TLS, GB-RAR and wind tower (b). The slant ranges $R_{TS,TLS}$ and $R_{TS,GB\text{-}RAR}$ of TLS and GB-RAR with respect to the TS are indicated, along with the slant distances $R_{TS,WT\text{-}B}$ and $R_{TS,WT\text{-}T}$ of the base and top of the wind tower. The TS survey makes it possible to compute the coordinates of each point P of the tower, in the same local reference system, and hence their slant ranges $R_{P,TLS}$ and $R_{P,GB\text{-}RAR}$ with respect to the TLS and GB-RAR. The topographic survey is not necessary if the entire structure can be surveyed by the TLS, which in this case allows us to obtain, along with the mutual positioning of the structure and GB-RAR, a 3D model of the structure and of the surrounding environment.

Figure 3 displays a high-resolution 3D digital model of the tower provided by the TLS with the slant ranges $R_{P,GB\text{-}RAR}$ and $R_{P,TLS}$. As a result, the spatial co-registration of TLS and GB-RAR measurements is obtained in a seamless way, taking into consideration the different spatial resolutions of TLS and GB-RAR measurements. Figure 4 shows the TLS measurements points mapping the shape

of the wind tower and the points corresponding to the center of each of 0.75 m-resolution cell of the GB-RAR. For each range cell of GB-RAR data, the corresponding TLS measurements are easily identified and compared or merged with GB-RAR data. The co-registration of the data in time is provided by a synchronization of TLS and GB-RAR acquisitions.

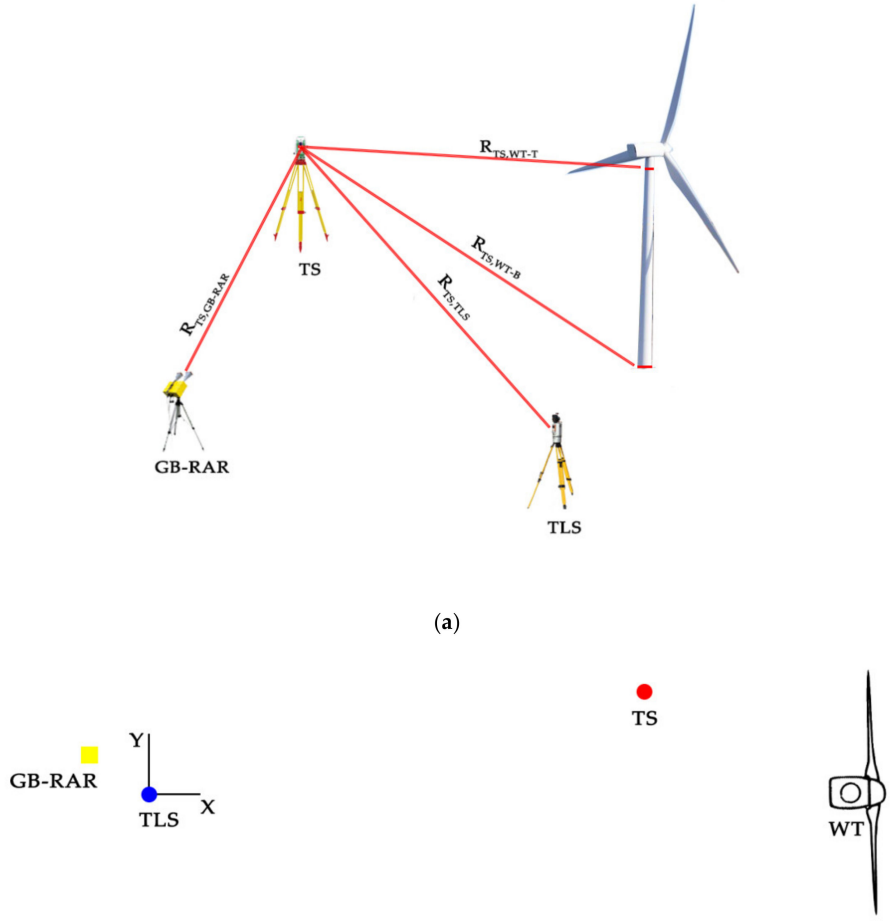


Figure 2. The TS survey layout with slant distances of TLS, GB-RAR, top and bottom of wind tower (**a**); The local reference system (TLS centered) used to co-locate TLS and GB-RAR measurements (**b**).

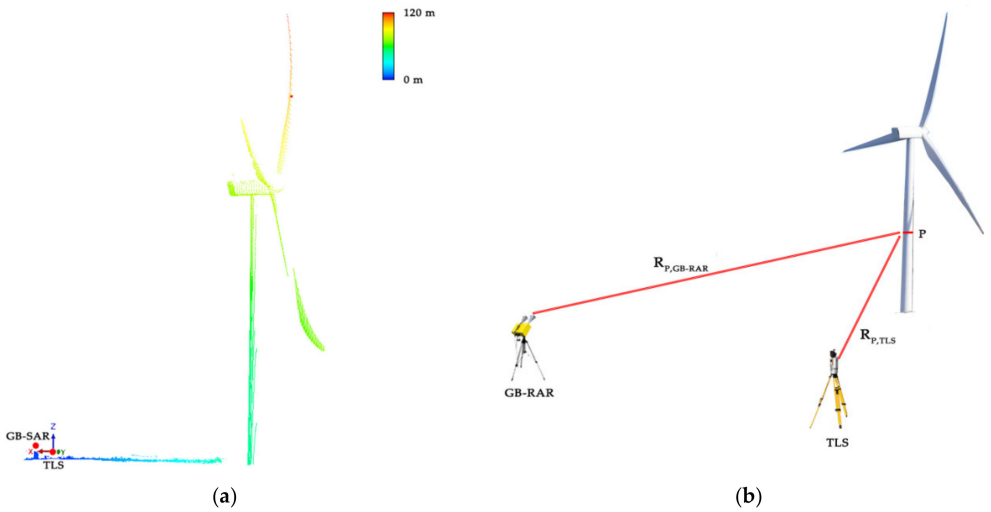


Figure 3. 3D digital surface model of the wind tower (**a**); The distances RP, GB-RAR and RP, TLS of point P on the tower with respect to TLS and GB-RAR (**b**).

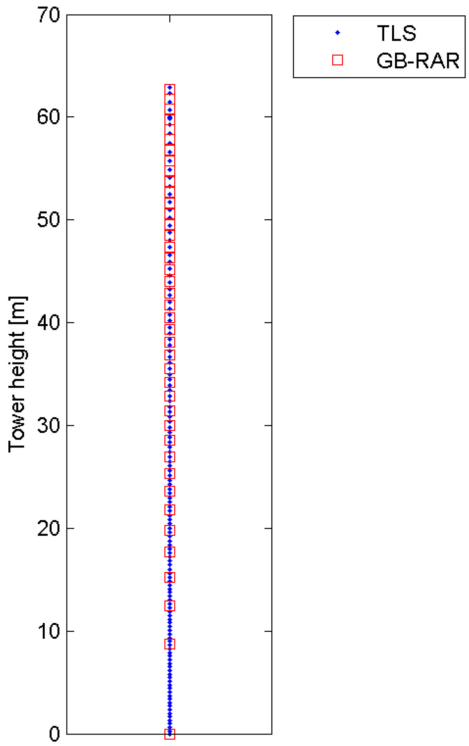


Figure 4. TLS (**blue dots**) and GB-RAR (**red square**) measurement points along the wind tower. The range distance and resolution of each GB-RAR measurement point is given by Equation (2).

2.3.2. Model-Based Processing of TLS Data and Estimation of Oscillation Amplitude and Frequency

Model-based processing of TLS data is widely used to determine with high precision the position of points materialized through known geometries. A typical example is given by the targets (spherical, cylindrical or plane) used for the registration of the scans carried out for the surveying of a 3D object [24,25].

If a stable target having a known geometry is surveyed, the parameters of the fitting surface corresponding to this geometry can be estimated from the cloud of n points acquired during the scan, through a least-squares procedure. The RMS of surface fit residuals exhibits a linear trend as a function of sampling resolution, i.e., of the square root of the number n of sampled points [26]. The deviations between the fitting surfaces, obtained from different scans of the same target, are proportional to $n^{-1/2}$ and, therefore, drastically lower than the single point precision of the instrument.

The model-based processing, in our case, is based on the use of interpolation to reduce noise and increase the precision of displacement measurements [20]. This approach is particularly suited for linear structures such as wind towers. In [19] the authors showed that, using an interpolating curve, the precision achieved in measuring the deformation of a beam can be 20 times higher than that of a single point. These conclusions had been confirmed in [27,28]. The knowledge of the geometry of the wind tower shown in Figure 3a is needed. A wind tower is a truncated cone with a circular section and a decreasing diameter upwards. Therefore, a generatrix is a straight line. The elastic line is certainly a continuous curve with a continuous derivative; in static conditions, for a load applied to the free end, it can be approximated by a third-order polynomial [29]. It is worth noting that the lines scanned by the VZ-1000 in line scanner mode do not belong to the same vertical plane, due to an imperfect orthogonality between the emitted laser beam and the rotation axis of the multi-facet mirror. This can also be inferred by observing the different horizontal angle associated with each scanned point. The laser beam would describe a conic section on a vertical surface instead of a straight line, as in the classic case of the theodolite line-of-sight, not orthogonal to the secondary axis. Given the size of the misalignment, there is a maximum deviation of about 0.4 m at the top of the tower compared to

the average generatrix. In any case, this effect does not affect the results obtained, since they are based on the differences between the scanned lines, which have the same deviation. To take into account these effects without making the calculation too heavy, the trace of the laser beam on the tower is approximated by a fourth-order polynomial in a (D,H)-plane, where D is the ground distance from the TLS and H is the height from the tower base. The following procedure is adopted for each line scan: (a) computation of coordinates of points of the TLS scanned line; (b) estimation of interpolating polynomial coefficients; (c) shift of the polynomial curve in order to make it pass through the base of the tower; (d) computation of the distance D for each selected height H along the tower.

Figure 5 shows the polynomial fitting of the points of a single line scan along the tower. The procedure is repeated for all the TLS scanned lines. This provides the distance D(H,t), of a point P with a height H at the acquisition time $_t$ and hence the time series of the distance D of point P with respect to the TLS. Time series are used to obtain the amplitude of the oscillations. As a final step, the wind tower's vibration frequencies are obtained by a spectral analysis.

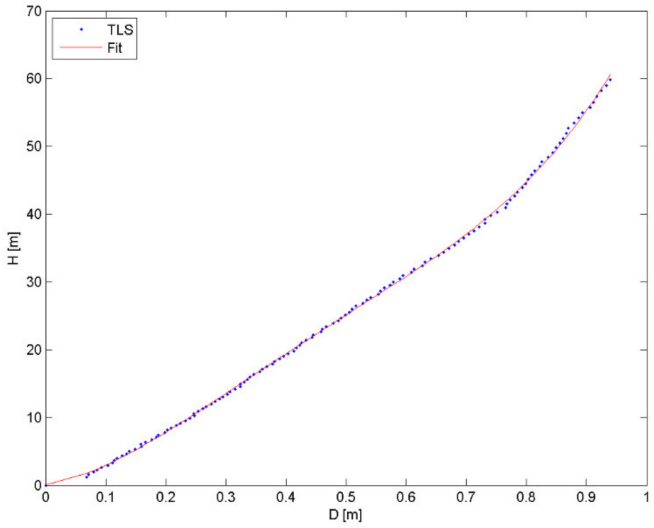


Figure 5. Polynomial fitting of points along the wind tower of a single line scan.

2.3.3. Interferometric Processing of GB-RAR Data and 2D Visualization of Oscillation Frequency Spectra

The stack of complex-valued GB-RAR acquisitions is processed by means of the interferometric radar technique by computing the phase differences of each pixel with respect to the first GB-RAR acquisition. The phase is first unwrapped and then mapped to propagation delay. Hence, the contribution of delay due to propagation in the atmosphere is modelled and removed, resulting in the measurement of the range $R_{P,GB\text{-}RAR}$ between the GB-RAR location and a target on the wind tower. A spectral analysis of the stack of range vectors $\{R_{P,GB\text{-}RAR}(t)\}_{P \epsilon TOWER}$, results in the 2D spectrum of the vibration frequencies. This procedure has been described in [18] and applied to the monitoring of bell-towers and monuments in [30]. An important step of the adaption of the estimation of the GB-RAR estimation of vibration frequencies to the study of the characterization of the dynamical properties of a wind tower is the co-registration of TLS and GB-RAR spectra as sketched in Figure 6. After co-registering TLS and GB-RAR measurements, it is possible to compare vibration spectra obtained by TLS and GB-RAR by a spectral analysis of the time series of distances. It is worth noting that due to the different spatial resolutions of TLS and GB-RAR data, more TLS spectra correspond to the a given frequency spectrum provided by GB-RAR interferometry. In fact, a GB-RAR range resolution of 0.75 m corresponds to a coarser spatial resolution along the wind tower, depending on the radar looking angle and the antenna irradiation pattern (Figure 4).

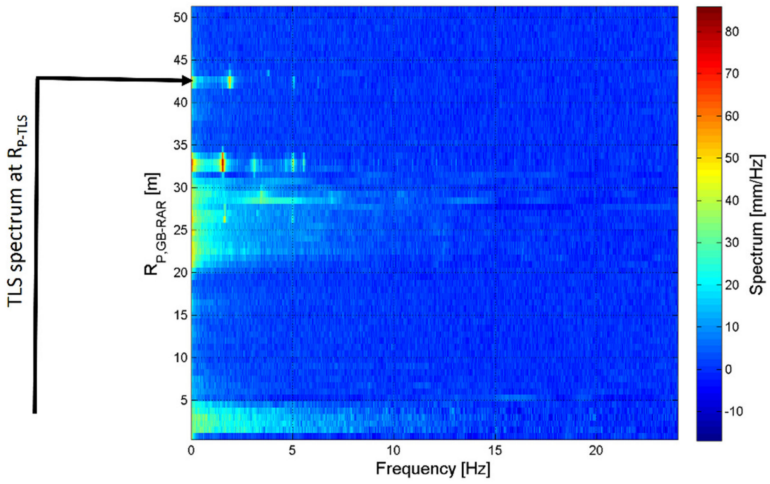


Figure 6. Sketch of proposed methodology to estimate vibration frequencies by the joint use of TLS and GB-RAR techniques.

3. Test and Results

This section summarizes the results obtained in the experimental test. It includes two subsections: Section 3.1 describes the case study and the measurement set up. Section 3.2 shows the results obtained by the proposed methodology.

3.1. Case Study

For the case study, a wind farm was chosen located in Tarsia, Southern Italy. Figure 7 displays the geographical location (a), an aerial Google© image (b) and a photo of the wind farm (c).



Figure 7. Google© images of the study area: (**a**) geographic position; (**b**) wind farm area (the investigated tower is circled in red); (**c**) panoramic view.

The wind farm is made up of 22 2.0 MW wind turbines, mounted on 65 m tall towers. The turbines are Gamesa® G90, characterized by a three-blade rotor and a diameter of ϕ = 90 m. The swept area is A = 6362 m^2 and the cut-in wind speed is v = 3.0 m/s. The tower has a truncated cone shape, the diameter is ϕ_b = 4.034 m at the base and ϕ_t = 2.314 m at the top; the height is H = 65 m.

The monitored wind tower is located at the most eastern side, where on the acquisition day the wind speed was greater than the threshold of v = 3 m/sec necessary to activate the wind turbines. The wind direction was almost constant during data acquisition, with a prevalent direction from the north-east, with an azimuth angle of 69°. The rotations of the nacelle during the data acquisition reached a maximum value of 5°, so they had no appreciable effect on the results.

A topographic survey was carried out in order to obtain a local reference system for all acquisitions. The survey made it possible to have a single reference also for the heights; zero was fixed at the base of the tower, not visible from the TLS and the GB-RAR up to the height of 1.80 m. For the alignment of the acquisitions, a TS Leica TP 1201+®, Leica Geosystem AG, Heerbrugg, Switzerland (angular accuracy 1", distance accuracy ± 1 mm ± 1 mm/km) was used. The acquisitions from TLS and GB RAR were carried out simultaneously, from 12.30 to 14.10 Central European Time (CET) on 17 July 2019.

The TLS, in line scanner configuration, was placed with the main axis vertical, so that the zenith angles of the laser beam varied between 30° and 130 °. The maximum scan speed of 120 lines/sec. was selected. The time taken per scan is 3.326×10^{-3} sec, while the time between two consecutive lines is 8.324×10^{-3} sec, with a time gap of 4.998×10^{-3} sec due to the geometry of the multi-facet mirror. The time taken to scan the only tower is 1.126×10^{-3} sec. Each line scanned describes a section comprising the wind tower and the ground between the TLS and the tower. Each TLS scan line provides a set of 140 point-like distance measurements, covering the whole tower. Given the scan speed of 120 lines per second, several thousand lines were acquired for each acquisition session. For the processing of the lines, measurement points near the connection of the nacelle were excluded to avoid outliers due to the pitch motion. The best-interpolating polynomial was obtained using the procedure described in Section 2.3.2. At this point, for a given height, it was possible to compute the value of the horizontal distance from the TLS for each line, approximately every 8 msec. The positions of the points on the same line, given the line scan time of about 1 msec, can be considered contemporary.

GB-RAR data were acquired using an elevation angle of 10° and antennas with a main irradiation lobe having an aperture of 39° in elevation and 11° in azimuth. As for time synchronization, the TLS is equipped with a GPS receiver, which makes it possible to convert timestamps to Central European Time (CET). For GB-RAR, the recorded acquisition time was converted using the CET provided by the operating system of the computer used as a data logger.

Acquisitions were made under various operating conditions of the wind turbine: (a) fully operational with the turbine active; (b) during the deactivation of the turbine; (c) during the stop without the action of the wind; (d) during the restart; (a) once again fully operational after the restart. Table 3 shows the start and end times for the seven acquisitions performed, the corresponding timestamps, and the operating conditions.

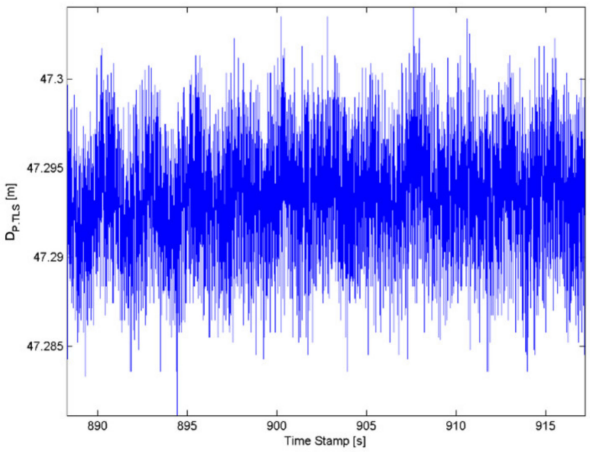
Table 3. TLS sampling periods.

Operating Condition	Initial Timestamp	Final Timestamp	Initial Time (CET)	Final Time (CET)
a	408.67	430.35	13.37.50	13.38.12
a	664.55	678.75	13.41.57	13.42.11
a	736.23	754.69	13.43.08	13.43.27
b	766.81	846.19	13.43.39	13.44.59
c	888.28	917.17	13.45.41	13.46.10
d	937.18	1054.41	13.46.29	13.48.27
a	643.17	708.68	14.00.00	14.01.06

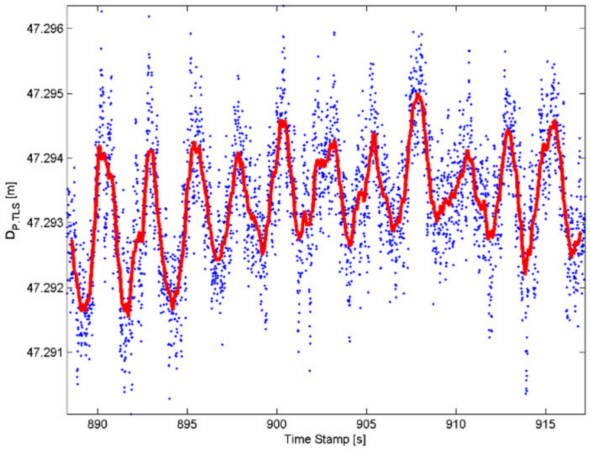
3.2. Results

Acquisitions corresponding to operating condition c (rotor blades motionless, no action of the wind) were used to obtain the mean value of the horizontal distance from TLS. For a point P on the wind tower located at H = 65 m height from the tower base, the mean ground distance of D = 47.293 m was

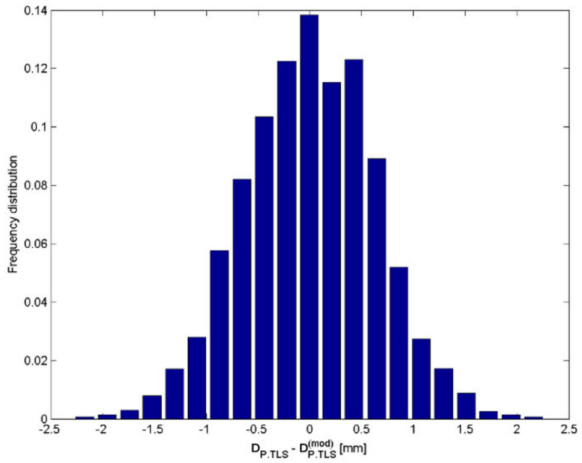
obtained. The procedure described in the Section 2.3.2 was applied. The comparison between raw data and the values obtained by the procedure can be observed in Figure 8.



(**a**)



(**b**)



(**c**)

Figure 8. (**a**) Distance DP,TLS of point P on the wind tower located at H = 65 m during acquisition in operating condition c (see Table 3); (**b**) result after applying the proposed methodology; (**c**) frequency distribution of differences between modelled DP,TLS distances (blue dots) and moving average (red line). The standard difference between measured and model DP,TLS distances is 0.6 mm.

The time series of TLS distances of point P, located at the top of the wind tower, is plotted in panel 8(a). Panel 8(b) displays the results obtained by applying the procedure in Section 2.3.2 to the detrended measurements of Panel 8(a). Results provided by the proposed methodology and the mean curve obtained by applying a moving average operator are plotted in Figure 8b, while the frequency distribution of their differences is plotted in Figure 8c. The standard deviation of this frequency distribution provides the precision of TLS estimates of distances equal to 0.6 mm.

Figure 9 shows the plot of TLS ground distances vs. timestamps of four points P on the wind tower located at different heights above the base, obtained by the proposed procedure. Data were collected from 13.41.57 till 13.42.11 CET. These results were obtained in condition a (see Table 3) with a fully operational wind turbine. The peak-to-peak amplitude of oscillations decreased from 15 mm to 2 mm when moving from H = 60 m to H = 15 m on the wind tower.

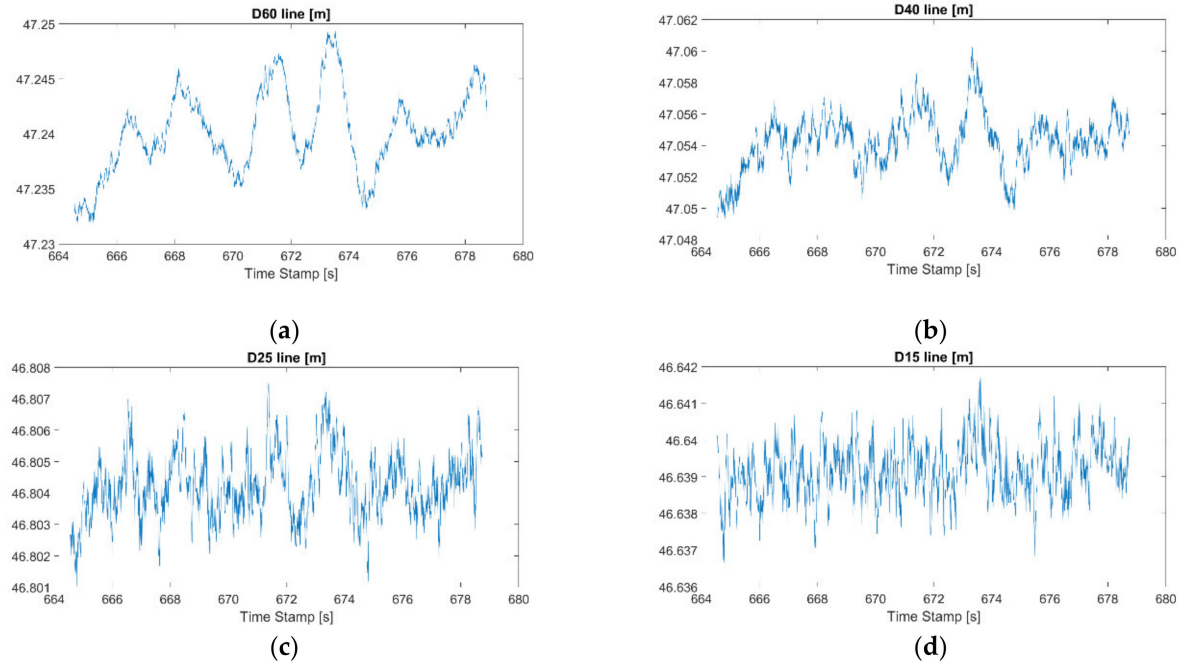


Figure 9. Ground distances from TLS of points at a height of 60 m (d_{60} line), 40 m (d_{40} line), 25 m (d_{25} line) and 15 m (d_{15} line) on the tower base. Abscissae are the timestamps in sec. The wind turbine is fully operational.

Figure 10 shows the plot of TLS ground distances vs. timestamps of a point P on the wind tower located at H = 60 m above the base. Data were collected from 13.43.39 till 13.44.59 CET. These results were obtained in condition b (see Table 3) with the wind turbine in deactivation mode. Damped oscillations had an amplitude decreasing from 90 mm to a few mm. The average ground distance from the TLS increased and tended to stabilize around a value of 47.293 m.

The corresponding spectrum of vibration frequencies are shown in Figure 11a,b, along with the spectrum obtained for data collected during the stop of the wind turbine in Figure 11c,d. In both cases, two peaks are observed at 0.4 Hz and 40 Hz.

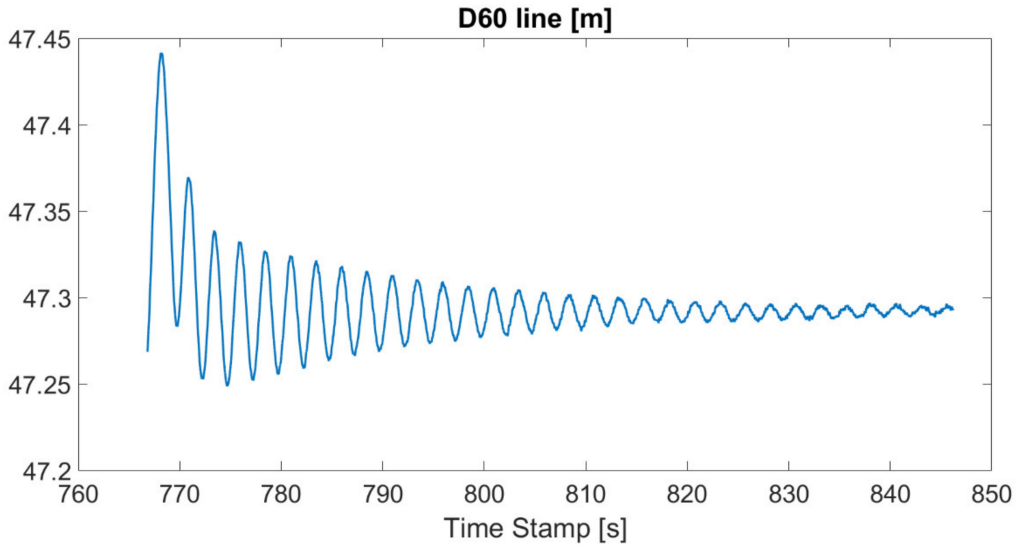


Figure 10. Ground distance D_{60} line from TLS of a point 60 m high on the tower base during the deactivation of the turbine.

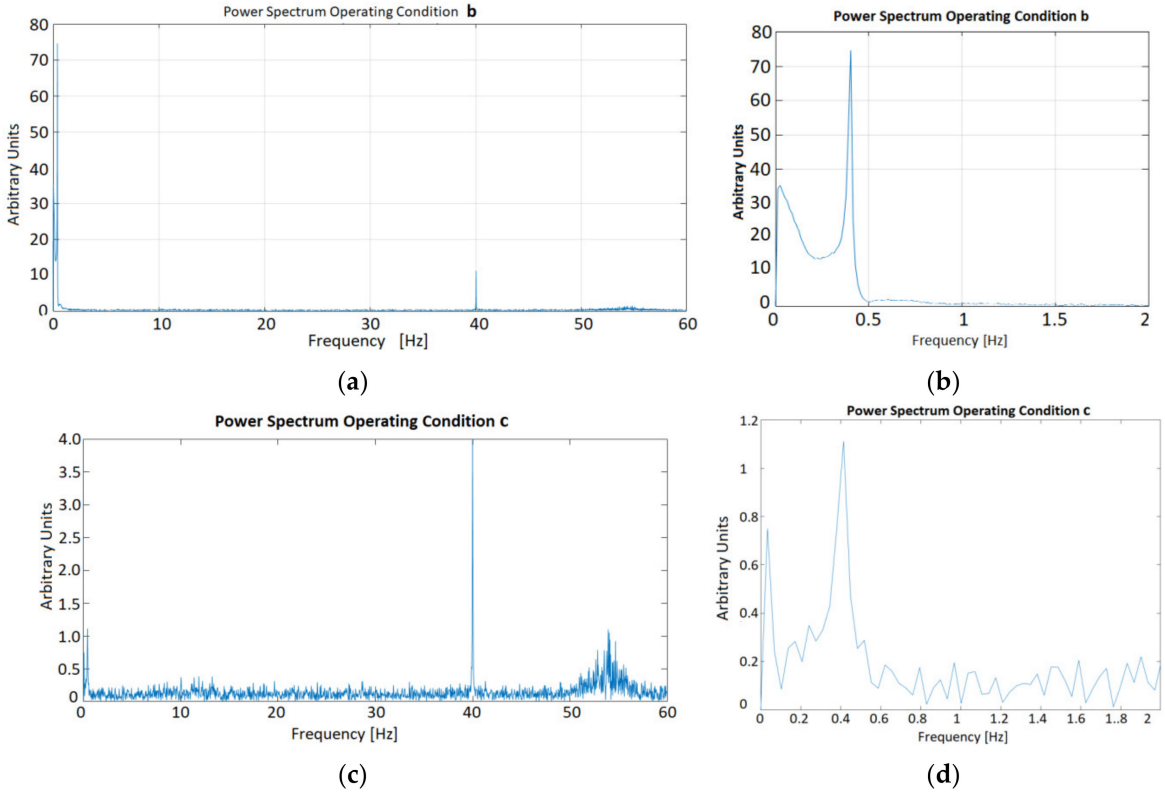
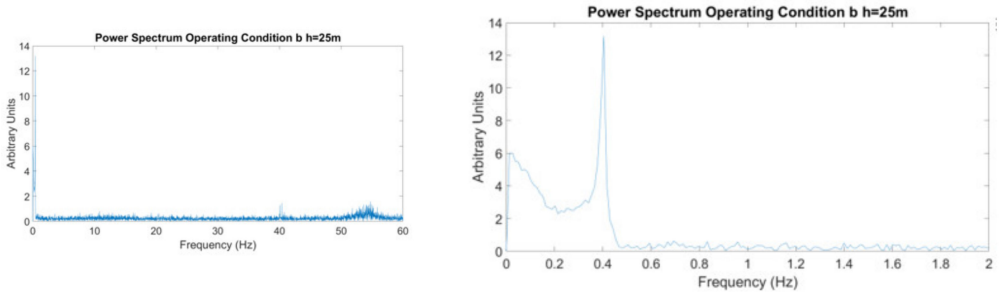


Figure 11. Spectra of vibration frequencies of point P on the wind tower located at H = 60 m. Spectrum for the data collected during the deactivation of the wind turbine (**a**). Enlargement of the low frequencies (**b**). Spectrum for the data collected during the stop of the wind turbine (**c**). Enlargement of the low frequencies (**d**).

Figure 12 shows the spectrum of vibration frequencies for a point P on the wind tower located at H = 25 m above the base, obtained for data collected during the deactivation of the wind turbine. Additionally, in this case, two peaks can be observed at 0.4 Hz and 40 Hz.



(**a**) (**b**)

Figure 12. Spectrum of vibration frequencies of point P on the wind tower located at H = 25 m. Data have been collected during the deactivation of the turbine (**a**). Enlargement of the low frequencies (**b**).

The spectrum of vibration frequencies obtained by processing GB-RAR data acquired during the stop of the wind turbine is reported in Figure 13. The spectrum refers to a point located at a height H = 25 m above the tower base, corresponding to a slant distance R = 54 m from the radar. Two peaks are observed at 0.4 Hz and 3.1 Hz. It worth noting that besides the common peak at frequency f = 0.4 Hz, the two spectra had different characteristics. In particular, it should be noted that the peak at f = 0.4 Hz measured by GB-RAR in operating condition c was measured by TLS at H = 60 m but not at H = 25 m. Probably, this was due to the different amplitude of oscillations at the top and bottom of the tower.

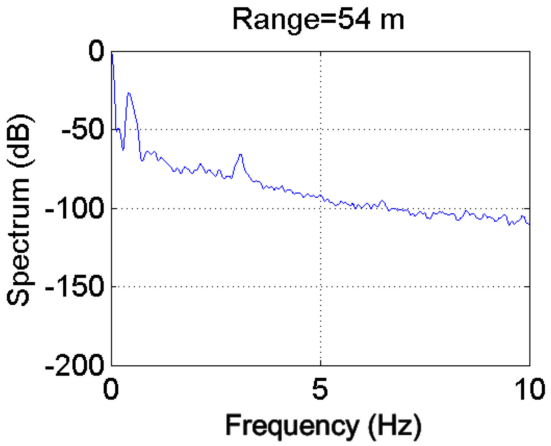


Figure 13. Spectrum of vibration frequencies of point P on the wind tower located at H = 25 m. Data have been collected during the stop of the turbine.

4. Numerical Analysis and Discussion

This section discusses the results presented in Section 3.

4.1. Evaluation of Displacements Due to the Wind

During the test, anemometric data were acquired, which showed a constant wind direction. The wind speed data make it possible to obtain the thrust on the tower. Given the geometric and mechanical characteristics of the tower, it was possible to calculate the displacements of the points at various heights. The wind pressure can be obtained by the Bernoulli Equation:

$$p = \frac{1}{2}\rho v^2 \tag{5}$$

where:

p = is the wind pressure [N/m^2]

ρ = air density [kg/m^3]
v = air speed [m/sec]

The air pressure, applied to the swept area of the rotor, must be multiplied to a coefficient less than 0.6 due to the Betz limit [31]. In our case, given the low wind speed, which implies a non-optimal rotor efficiency, we can use the value 0.4. It is also necessary to take into account the interference factor b (i.e., the ratio of the downstream speed v_2 to the upstream speed v_1, which in our case can be considered equal to 0.577 [32]). Given that the speed measured by the anemometers and used for our test (installed on the nacelle and behind the rotor) is the downstream speed, the thrust F acting on the top of the tower, considered as a cantilever, can therefore be evaluated as [32]:

$$F \cong 0.4\left(\frac{1}{2}\rho 3 v_2^2 \pi r^2\right) = 0.60\left(\rho v_2^2 \pi r^2\right) \tag{6}$$

where r is the radius of the rotor. Geometric and material data on the tower can be found in [33]. The displacement δ at the top of the tower, in correspondence of the connection with the nacelle, is obtained by:

$$\delta = F\frac{L^3}{3EJ} \tag{7}$$

where:

L = cantilever length
E = Young's modulus
J = moment of inertia

For our calculations, we assumed ρ = 1.2 kg/m^3, L = 65 m, E = 2.1×10^{11} N/m^2, J = 0.323 m^4. Actually, the lowering changes with the wind speed, and other effects affect the final results, so only a rough estimate can be obtained with Equation (7). Table 4 shows the displacements of a point 65 m high on the base of the tower computed for different wind speeds. By adding to the displacements, the mean value of the ground distances measured in the operating condition c, i.e., during the stop of the rotor blades, one can obtain the ground distances from TLS for the tower subject to the wind load.

Table 4. Theoretical displacements.

Wind Speed [m/s]	Thrust [N]	E [N/m^2]	J [m^4]	L [m]	Displacement d [m]
2	18,321	2.1×10^{11}	0.323	65	0.0247
2.5	28,627	2.1×10^{11}	0.323	65	0.0387
3	41,223	2.1×10^{11}	0.323	65	0.0557
3.5	56,109	2.1×10^{11}	0.323	65	0.0758
4	73,285	2.1×10^{11}	0.323	65	0.0990
4.5	92,751	2.1×10^{11}	0.323	65	0.1253
5	114,508	2.1×10^{11}	0.323	65	0.1547

4.2. Numerical Analysis of Natural Frequencies

This section provides a simple numerical analysis for the computation of natural frequencies of a cantilever subject to free oscillations. An approximated value of the circular natural frequencies, in case of a fixed cross section, is given by [34]:

$$\omega_n = \alpha_n^2 \sqrt{\frac{EJ}{mL^4}} \tag{8}$$

where:

ω_n = n-th circular natural frequency
α_n = 1.875, 4.694, 7.885

E = Young's modulus
J = moment of inertia
m = mass per length unit
L = cantilever length

The natural frequency f_n can be obtained from the circular frequency using the equation:

$$f_n = \frac{\omega_n}{2\pi} \tag{9}$$

To bring back the problem to the case of a massless cantilever with a discrete effective mass applied to the free end, we use the effective mass for the n-th frequency $m_{\mathrm{eff}}^{(n)}$, given by:

$$m_{eff}^{(n)} = \frac{3EJ}{L^3\omega_n^2} \tag{10}$$

This way we can add a m_{end} mass actually positioned at the free end of the cantilever and consider a total mass M_n at the free end:

$$M_n = m_{eff}^{(n)} + m_{end} \tag{11}$$

The n-th natural frequency will be:

$$\omega_n = \alpha_n^2 \sqrt{\frac{3EJ}{M_n L^4}} \tag{12}$$

In our case, given the characteristics of the tower, its mean section and the wind turbine data [33] we can assume E = 2.1×10^{11} N/m^2, J = 0.322 m^4, m = 2800 kg/m, L = 65 m. By using Equations (9) and (10), we obtain a discrete effective mass of 40,740 kg for the first frequency and of 1120 kg for the second one. We must add the weight of rotor and nacelle, equal to about 8×10^4 kg. By using Equations (11) and (12), we get, for the first three natural frequencies, the values f_1 = 0.394 Hz, f_2 = 3.10 Hz, f_3 = 8.596 Hz, and the relevant periods T_1 = 2.54 sec, T_2 = 0.32 sec, and T_3 = 0.11 sec.

4.3. Measured vs. Theoretical Displacements

In the following, we consider the oscillation amplitudes of a point located at H = 65 m above the base of the tower. The choice of a point near the top of the tower allows us to consider displacements of greater amplitude. This is also useful, given the wind speed, which was not high during the test. Figure 14 shows the wind downstream speed during the test. The wind direction was constant during data acquisition.

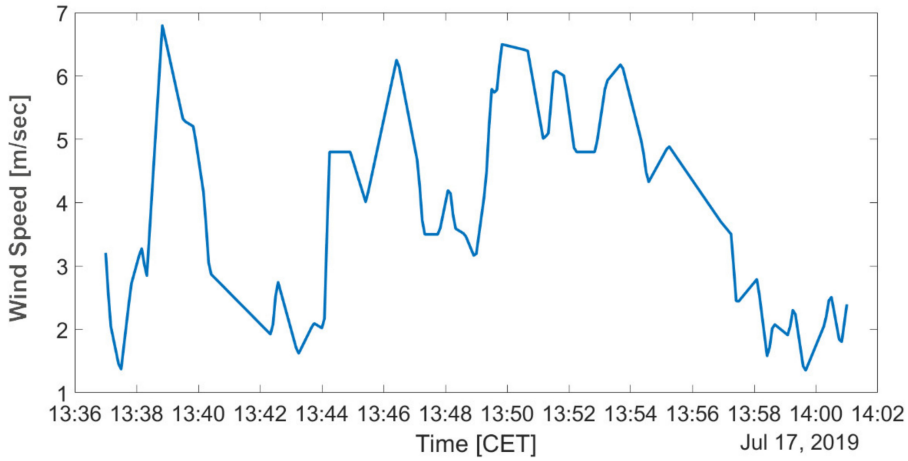


Figure 14. Wind speed in m/sec (downstream) measured by the wind turbine anemometers during the test.

In Table 5 we can see a comparison between the values of the theoretical ground distances and the values measured by TLS in different acquisitions. The theoretical distances have been obtained by subtracting the computed displacements to the mean ground distance D = 47.293 m, obtained in case of motionless rotor blades (see Figure 8a and condition c in Table 3).

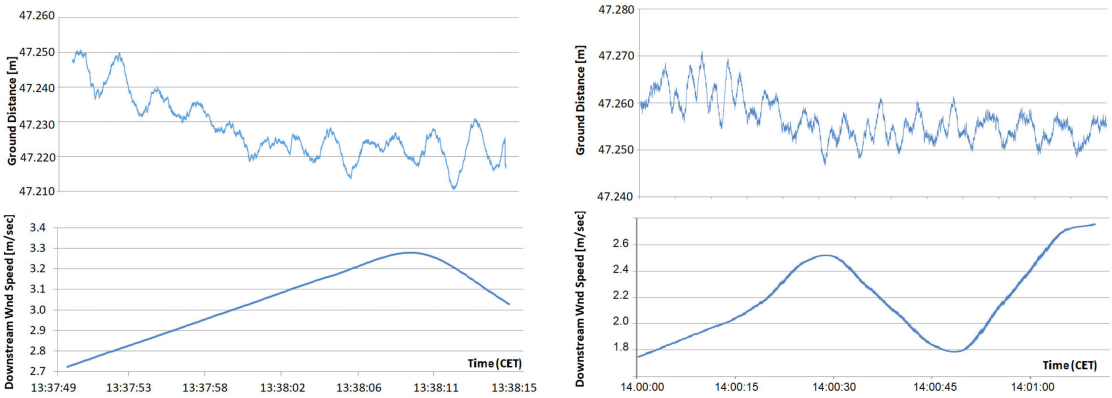
Table 5. Theoretical and measured ground distances from TLS of a point 65 m high.

Start Time [CET]	End Time [CET]	Wind Speed [m/sec] min	Wind Speed [m/sec] max	Measured D [m] min	Measured D [m] max	Theoretical D [m] min	Theoretical D [m] max
13.37.50	13.38.12	2.72	3.25	47.247	47.225	47.247	47.227
14.00.00	14.01.06	2.20	2.40	47.262	47.255	47.260	47.254

Figure 15 shows the displacements of the considered point during the activity of turbine. In the lower part of the figure, the wind speed is represented. Acquisition times are synchronized (see Table 3); the wind direction was constant.

It can be observed that the increase in wind speed leads to a greater deformation and, therefore, to an approach of the point to the TLS located on the opposite side of the rotor. The deformation values δ obtained are in accordance with those obtained with Equation (7).

A continuous oscillation of the point is observed which has a period of around two seconds. This value is not constant and is affected by the noise of the measurements, as well as by the variability of the wind thrust. The amplitude of the oscillations varies from 10 to 20 mm.



(**a**) (**b**)

Figure 15. Ground distance from TLS of a point P on the tower located at H = 65 m during the activity of the turbine, from 13:37:50 to 13:38:12 (**a**) and from 14:00:00 to 14:01:06 (**b**). Below the graphics of the distances, the wind speed in m/sec. X axis is the time, both for upper and lower figures.

4.4. Measured vs. Theoretical Frequencies

In this section, we discuss the properties of the measured vibration spectra and compare them to the theoretical analysis of the wind tower reported in Section 4.2. The 0.4 Hz frequency measured by both TLS and GB-RAR is in agreement with the value obtained using the analytical formulas for the first natural frequency. The frequency f = 3.1 Hz of the second oscillation mode is measured by GB-RAR but not by TLS, probably due to lower precision of TLS when compared to GB-RAR.

The frequency peak at f = 40 Hz found in all TLS measurements is an artifact due to the rotating mirror. In fact, the laser beam used for measurements in the TLS VZ1000 is addressed and collected by a rotating three-sided mirror, i.e., by the lateral faces of a triangular-based prism. When a scan speed of 120 lines per second is selected, the three-sided mirror rotates with an angular speed of 40 revolutions per second. Even a slight vibration of the rotation axis can cause oscillations in the results at a frequency

of 40 Hz (Figure 16a). To confirm this hypothesis, the results of the measurements performed with a slower scanning speed of 60 lines per second were analyzed.

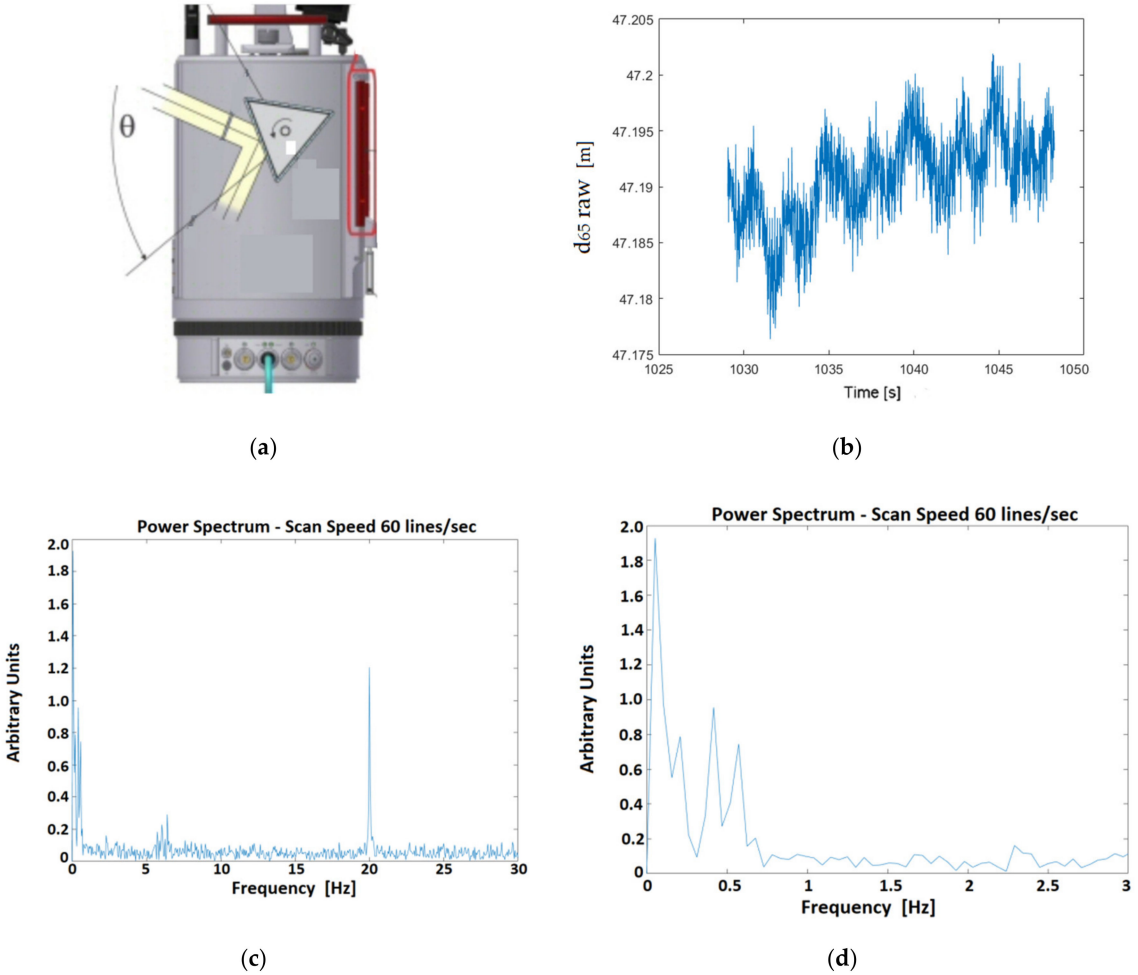


Figure 16. The scheme of rotating mirror of VZ1000 TLS (**a**). Ground distance from TLS of a point 65 m high on the tower base during the acquisition with scan speed 60 Hz (**b**). Power Spectrum obtained by FFT for the ground distance from TLS (**c**). Enlargement of Figure 16c (**d**).

Figure 16b shows the displacements of a point 65 m high on the tower base during the acquisitions. Figure 16c shows the power spectrum for the ground distance from TLS of a point 65 m high on the tower base. Two peaks are present: the first at a low frequency, the second at 20 Hz. In Figure 16d the first peak is enlarged, corresponding to a frequency of 0.4 Hz. The results confirm the above hypothesis, so we can attribute the peak at the highest frequency to the vibration of the rotating mirror of the TLS.

5. Conclusions

A methodology has been proposed for measuring the vibration frequencies and the amplitude of the oscillations of tall structures by joint use of TLS and GB-RAR. The methodology exploits the possibility of using a TLS in line scan mode, thus extracting a large number of scan lines per second. The use of lines interpolating the individual scanned points makes it possible to obtain results with a precision better than that of the instrument. For a given point on the structure, the stack of TLS lines is used to derive the temporal profile of displacements and from this the spectrum of vibration frequencies. It has been observed the TLS estimate of vibration frequencies is limited by the precision of displacement measurements. For oscillations whose amplitude is much smaller than the TLS precision, the proposed methodology based on TLS data cannot estimate the vibration frequency. This problem

is overcome by the joint use of co-located GB-RAR. The higher precision of GB-RAR measurements of tower displacements provides vibration frequencies corresponding to smaller oscillation amplitudes.

Results provided by the proposed methodology based on the joint use of co-located TLS and GB-RAR systems have been compared to the output of a numerical analysis of tower displacements, modelling the tower as subject to a wind load derived from the anemometric data.

The comparison of results obtained by the numerical analysis and measurements leads to the following conclusions: (a) the proposed processing technique based on the geometrical modelling of the structure can enhance the precision of distance measurements below the 5 mm declared for the TLS instrument; (b) the joint use of co-located TLS and GB-RAR can provide richer information on the dynamical behavior of the structure, with the sub-centimeter spatial resolution of TLS, and on the whole spectral characterization of vibrations, including those having an amplitude much smaller than the TLS precision, thanks to the sub-millimeter precision of GB-RAR measurements.

The proposed methodology can be a useful and cheap support for non-contact inspection and monitoring of tall structures.

Author Contributions: Conceptualization, S.A.; methodology, S.A.; software, S.A. and G.N.; investigation, S.A. and G.N.; writing—original draft preparation, S.A. and G.N.; writing—review and editing, S.A. and G.N. All authors have read and agreed to the published version of this manuscript.

Funding: This research received no external funding.

Acknowledgments: Authors acknowledge EON Italia Spa for support during data acquisition. The authors would like to thank the entire DIAN S.R.L. team for the acquisition and processing of GB-RAR data.

Conflicts of Interest: The authors declare no conflict of interest.

References

1. Zinno, R.; Artese, S.; Clausi, G.; Magarò, F.; Meduri, S.; Miceli, A.; Venneri, A. Structural Health Monitoring (SHM). In *The Internet of Things for Smart Urban Ecosystems*; Cicirelli, F., Guerrieri, A., Mastroianni, C., Spezzano, G., Vinci, A., Eds.; Springer International Publishing: Cham, Switzerland, 2019; pp. 225–249. [CrossRef]
2. Fan, W.; Qiao, P. Vibration-based damage identification methods: A review and comparative study. *Struct. Health Monit.* **2011**, *10*, 83–111. [CrossRef]
3. Carden, E.P.; Fanning, P. Vibration based condition monitoring: A review. *Struct. Health Monit.* **2004**, *3*, 355–377. [CrossRef]
4. Kim, D.H.; Feng, M.Q. Real-time structural health monitoring using a novel fiber-optic accelerometer system. *IEEE Sens. J.* **2007**, *7*, 536–543. [CrossRef]
5. Bui, Q.B.; Hans, S. Dynamic behaviour of an asymmetric building: Experimental and numerical studies. *Case Stud. Nondestruct. Test. Eval.* **2014**, *2*, 38–48. [CrossRef]
6. Sabato, A.; Niezrecki, C.; Fortino, G. Wireless MEMS-Based Accelerometer Sensor Boards for Structural Vibration Monitoring: A Review. *IEEE Sens. J.* **2016**, *17*, 226–235. [CrossRef]
7. Artese, G.; Perrelli, M.; Artese, S.; Meduri, S.; Brogno, N. POIS, a Low Cost Tilt and Position Sensor: Design and First Tests. *Sensors* **2015**, *15*, 10806–10824. [CrossRef]
8. Yu, J.X.; Meng, X.; Shao, X.; Yan, B.; Yang, L. Identification of dynamic displacements and modal frequencies of a medium-span suspension bridge using multimode GNSS processing. *Eng. Struct.* **2014**, *81*, 432–443. [CrossRef]
9. Lienhart, W.; Ehrhart, M.; Grick, M. High Frequent Total Station Measurements for the Monitoring of Bridge Vibrations. In Proceedings of the 3rd Joint International Symposium on Deformation Monitoring (JISDM), Vienna, Austria, 30 March–1 April 2016; Available online: https://www.fig.net/resources/proceedings/2016/ (accessed on 2 September 2019).
10. Artese, S.; Perrelli, M. Monitoring a Landslide with High Accuracy by Total Station: A DTM-Based Model to Correct for the Atmospheric Effects. *Geosciences* **2018**, *8*, 46. [CrossRef]
11. Xu, Y.; Brownjohn, J.M.W. Review of machine-vision based methodologies for displacement measurement in civil structures. *J. Civ. Struct. Health Monit.* **2018**, *8*, 91. [CrossRef]
12. Artese, S.; Achilli, V.; Zinno, R. Monitoring of Bridges by a Laser Pointer: Dynamic Measurement of Support Rotations and Elastic Line Displacements: Methodology and First Test. *Sensors* **2018**, *18*, 338. [CrossRef]

13. Pieraccini, M. Monitoring of Civil Infrastructures by Interferometric Radar: A Review. *Sci. World J. Vol.* **2013**, 786961. [CrossRef] [PubMed]
14. Anghel, A.; Tudose, M.; Cacoveanu, R.; Datcu, M.; Nico, G.; Masci, O.; Dongyang, A.; Tian, W.; Hu, C.; Ding, Z.; et al. Compact Ground-Based Interferometric Synthetic Aperture Radar: Short-range structural monitoring. *IEEE Signal Process. Mag.* **2019**, *36*, 42–52. [CrossRef]
15. Nico, G.; Borrelli, L.; Di Pasquale, A.; Antronico, L.; Gullà, G. Monitoring of an ancient landslide phenomenon by GBSAR technique in the Maierato town (Calabria, Italy). *Eng. Geol. Soc. Territ.* **2015**, *2*, 129–133. [CrossRef]
16. Nico, G.; Cifarelli, G.; Miccoli, G.; Soccodato, F.; Feng, W.; Sato, M.; Miliziano, S.; Marini, M. Measurement of pier deformation patterns by ground-based SAR interferometry: Application to a bollard pull trial. *IEEE J. Ocean. Eng.* **2018**, *43*, 822–829. [CrossRef]
17. Di Pasquale, A.; Nico, G.; Pitullo, A.; Prezioso, G. Monitoring Strategies of Earth Dams by Ground-Based Radar Interferometry: How to Extract Useful Information for Seismic Risk Assessment. *Sensors* **2018**, *18*, 244. [CrossRef]
18. Atzeni, C.; Bicci, A.; Dei, D.; Fratini, M.; Pieraccini, M. Remote Survey of the Leaning Tower of Pisa by Interferometric Sensing. *IEEE Geosci. Remote Sens.* **2010**, *7*, 185–189. [CrossRef]
19. Gordon, S.J.; Lichti, D.D. Modeling Terrestrial Laser Scanner Data for Precise Structural Deformation Measurement. *J. Surv. Eng.* **2007**, *133*, 72–80. [CrossRef]
20. Kim, K.; Kim, J. Dynamic displacement measurement of a vibratory object using a terrestrial laser scanner. *Meas. Sci. Technol.* **2015**, *26*, 045002. [CrossRef]
21. Neitzel, F.; Niemeier, W.; Weisbrich, S.; Lehmann, M. Investigation of Low-Cost Accelerometer, Terrestrial Laser Scanner and Ground-Based Radar Interferometer for Vibration Monitoring of Bridges. In Proceedings of the Sixth European Workshop on Structural Health Monitoring, Dresden, Germany, 3–6 July 2012.
22. Schill, F.; Eichhorn, A. Investigations of low- and high-frequency movements of wind power plants using a profile laser scanner. In Proceedings of the Joint International Symposium on Deformation Monitoring JISDM 2016, Vienna, Austria, 30 March–1 April 2016.
23. Mukupa, W.; Roberts, G.W.; Hancock, C.M.; Al-Manasir, K. A review of the use of terrestrial laser scanning application for change detection and deformation monitoring of structures. *Surv. Rev.* **2017**, *49*, 99–116. [CrossRef]
24. Urbančič, T.; Roškar, Z.; Fras, M.K.; Grigillo, D. New Target for Accurate Terrestrial Laser Scanning and Unmanned Aerial Vehicle Point Cloud Registration. *Sensors* **2019**, *19*, 3179. [CrossRef]
25. Bolkas, D.; Martinez, A. Effect of target color and scanning geometry on terrestrial LiDAR point-cloud noise and plane fitting. *J. Appl. Geod.* **2017**. [CrossRef]
26. Lichti, D.D.; Glennie, C.L.; Jahraus, A.; Hartzell, P. New Approach for Low-Cost TLS Target Measurement. *J. Surv. Eng.* **2019**, *145*, 04019008. [CrossRef]
27. Artese, S. The Survey of the San Francesco Bridge by Santiago Calatrava in Cosenza, Italy. *Int. Arch. Photogramm. Remote Sens. Spat. Inf. Sci.* **2019**, 33–37. [CrossRef]
28. Artese, S.; Zinno, R. TLS for dynamic measurement of the elastic line of bridges. *Appl. Sci.* **2020**, *10*, 1182. [CrossRef]
29. Chen, W.F.; Lui, E.M. *Handbook of Structural Engineering*, 2nd ed.; CRC Press: Boca Raton, FL, USA, 2005; ISBN 9780849315695.
30. Nico, G.; Masci, O.; Panidi, E. Non-destructive monitoring strategies of historical constructions and tangible cultural heritage based on ground-based SAR interferometry. In Proceedings of the InterCarto/InterGIS, International Conference, Petrozavodsk, Russia, July 19–1 August 2018; Volume 24, pp. 528–535. [CrossRef]
31. Betz, A. The Maximum of the theoretically possible exploitation of wind by means of a wind motor. *Wind Eng.* **2013**, *37*, 441–446. [CrossRef]
32. Ragheb, M.; Ragheb, A.M. Wind Turbines Theory—The Betz Equation and Optimal Rotor Tip Speed Ratio. In *Fundamental and Advanced Topics in Wind Power*; Carriveau, R., Ed.; IntechOpen Limited: London, UK, 2011; ISBN 978-953-307-508-2. [CrossRef]
33. Gamesa G90. Available online: https://en.wind-turbine-models.com/turbines/763-gamesa-g90 (accessed on 20 January 2020).
34. Thomson, W.T. *Theory of Vibration with Applications*; Kindersley Publishing, Inc.: London, UK, 2007.



© 2020 by the authors. Licensee MDPI, Basel, Switzerland. This article is an open access article distributed under the terms and conditions of the Creative Commons Attribution (CC BY) license (http://creativecommons.org/licenses/by/4.0/).